Carbon Materials

DOI: 10.1002/anie.201207855

Assembly and Magnetic Bistability of Mn_3O_4 Nanoparticles Encapsulated in Hollow Carbon Nanofibers**

Maria del Carmen Gimenez-Lopez, Alessandro La Torre, Michael W. Fay, Paul D. Brown, and Andrei N. Khlobystov**

Next-generation spintronic and data storage devices will be based on nanoscale functional materials such as magnetic nanoparticles.[1] One particular challenge for harnessing the magnetic bistability, quantum tunnelling of magnetization, and quantum coherence[2] of nanometer-sized magnetic objects is their coupling to the macroscopic world. Hollow carbon nanostructures with one macroscopic and two nanoscopic dimensions provide excellent materials to achieve this coupling, through the encapsulation and confinement of magnetic species.[3,4]

The insertion of magnetic nanoparticles into carbon nanostructures has been achieved mainly through the sublimation of a metal precursor,[5] or the capillarity filling of a molten metal salt followed by pyrolysis of the encapsulated material.[6] The main drawback of these approaches is a lack of control over the composition, size, and morphology of the nanoparticles formed inside the nanotubes. Since the functional properties of nanometer-sized magnetic objects are strongly dependent on these parameters, precise methods for encapsulation are required.[7] The insertion of preformed nanoparticles with well-defined magnetic properties into carbon nanostructures, under conditions where their structures and properties are fully retained, could offer a powerful route for the development of novel architectures for spintronic devices.[8] To date, the encapsulation of preformed nanoparticles has been reported only for nonmagnetic metals.[9–11] Even though the size, shape, and composition of preformed nanoparticles can be effectively controlled by various preparation methods,[12,13] the control of nanoparticle assemblies and their associated properties, combined with their confinement within carbon nanostructures, still remains a challenge.

Here, we report the first example of the encapsulation of preformed, non-equiaxed, magnetic nanoparticles (NPs) within hollow carbon nanofibers (NFs), demonstrating the importance of the host-container internal structure on the NP assemblies and hence their collective magnetic properties.

Two different types of hollow carbon nanofibers with different internal surface morphologies were employed to investigate the effects of confinement on the NP assembly and magnetic properties of the resultant hybrid nanostructures. The first type, a herringbone carbon nanofiber (CNF), comprised individual graphene layers tilted with respect to the main axis of the nanofiber, forming a uniform infinite stack (Figure 1 A–C). The second type, a graphitized carbon nanofiber (GNF), comprised several graphene layers grouped together into short stacked assemblies with slight offset to each other along the GNF axis (Figure 1 D–F). In this case, each stack of graphene layers formed a 2–3 nm step-edge, which, in principle, could provide a site for strong interaction between the host-NF and guest-NP through van der Waals forces, in turn disrupting interparticle interactions, altering their relative orientations, and affecting the magnetic properties of the resultant composite material.[14]

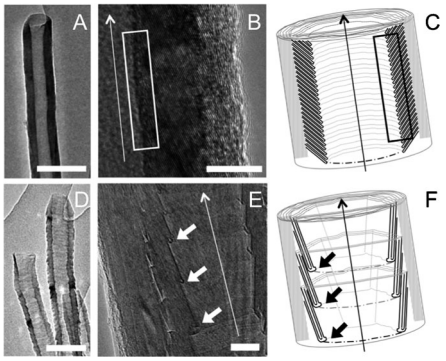

Figure 1. TEM images of host CNF (A,B) and GNF (D,E) showing their internal structures. Schematic representation of the CNF (C) and the herringbone GNF (F). The long arrows indicate the main axes of the nanofibers. The rectangular frames highlight the internal uniform graphitic layers of the CNF. The short arrows point to the internal step-edges of the GNF. The scale bars are 100 nm in (A) and (D), and 10 nm in (B) and (E).

[*] Dr. M. C. Gimenez-Lopez, A. La Torre, Prof. Dr. A. N. Khlobystov
School of Chemistry, Nottingham University, University Park
Nottingham, NG7 2RD (UK)
E-mail: Maria.Gimenez-Lopez@nottingham.ac.uk
Andrei.Khlobystov@nottingham.ac.uk
Dr. M. W. Fay
Nottingham Nanoscience and Nanotechnology Centre, University of Nottingham, University Park
Nottingham, NG7 2RD (UK)
Prof. Dr. P. D. Brown
Division of Materials, Mechanics and Structures, Department of Mechanical, Materials and Manufacturing Engineering, Faculty of Engineering, University of Nottingham
University Park, Nottingham NG7 2RD (UK)

[**] The authors acknowledge the financial support of the Royal Society (Dorothy Hodgkin Fellowship for M.C.G.-L. and University Research Fellowship for A.N.K.) and thank Dr. M. Clemente-León and J. M. Martinez-Agudo (ICMOL, University of Valencia) for assistance with the magnetic measurements.

Supporting information for this article is available on the WWW under http://dx.doi.org/10.1002/anie.201207855.

Oleylamine-stabilized manganese oxide (Mn_3O_4) was selected for these encapsulation experiments.[15] Indeed, nanometer-sized manganese oxide has attracted considerable attention as a result of its potential applications as catalyst,[16] supercapacitor,[17,18] and microwave-absorbing material.[19] High-resolution transmission electron microscopy (HRTEM) imaging shows a strong tendency of magnetic Mn_3O_4 "nanobricks" to self-assemble into highly ordered, two-dimensional, close-packed arrays on a flat amorphous carbon film (Figure 2A). IR spectroscopy and thermogravimetric analysis (TGA) indicated that oleylamine remained adsorbed on the NP surfaces of these 2D arrays[20] (see Figures S2 and S3 in the Supporting Information). In contrast to bulk Mn_3O_4, which is known to order ferrimagnetically at $T_N = 42$ K,[21,22] the Mn_3O_4 NPs exhibit ferromagnetic behavior at low temperatures,[23] with direct current (DC) magnetization measurements for these nanobricks showing a splitting of the field-cooled (FC) and zero-field-cooled (ZFC) responses below 45 K and a maximum of the ZFC signal at 35.2 K (Figure S4). Here, the shape of the magnetic contribution observed above 40 K is attributed to interparticle interactions, rather than to Mn_3O_4–MnO_2 core–shell interactions, as reported previously for equiaxed (spheroidal) NPs.[24] The large coercive field is attributed to shape anisotropy effects of the Mn_3O_4 nanobricks (Figure S6).[25] Further, alternating current (AC) susceptibility measurements showed a clear out-of-phase (χ'') signal, being a signature of slow relaxation of magnetization (Figures S7 and S8). The frequency dependence observed for the out-of-phase (χ'') signal is typical of interacting magnetic NPs and spin-glass systems.[26,27] These combined measurements suggest that the different stacking modes and orientations of Mn_3O_4 NPs within hollow carbon nanofibers should have a pronounced effect on their collective magnetic properties.

By immersing open and dry CNFs into colloidal suspensions of Mn_3O_4 NPs in an organic solvent (hexane), preformed Mn_3O_4 nanobricks were efficiently inserted into CNFs (mean length 3 μm and internal diameters of 30–60 nm) by capillarity forces. For insertion into longer GNFs (mean length 5 μm and internal diameters 30–100 nm), a colloidal suspension of Mn_3O_4 NPs in hexane diluted with supercritical CO_2 (4000 psi, 40 °C) was employed to minimize the transport resistance arising from the viscosity of conventional solvents. TEM investigation of the resultant hybrid nanostructures, being the first example of non-equiaxed preformed NPs encapsulated into carbon nanostructures, showed that Mn_3O_4@CNF (Figure 3A–D) contained highly aggregated guest-NPs within the smooth cavities of the CNFs, whereas in Mn_3O_4@GNF (Figure 3E–H) the guest-NPs were trapped at the internal step-edges, well dispersed, and distributed throughout the GNF container as discrete NPs (Table 1). These observations are in agreement with the higher loading of Mn_3O_4 within Mn_3O_4@CNF (26%) compared to Mn_3O_4@GNF (11%) as revealed by TGA (Figure S12). As

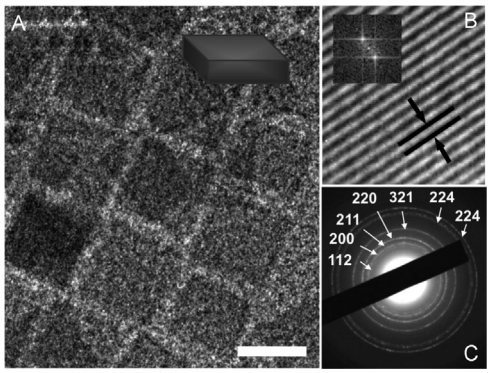

Figure 2. A) TEM image of a close-packed array of oleylamine-stabilized Mn_3O_4 nanobricks (with side dimensions of 11.4 ± 1.6 and 10.1 ± 1.5 nm and thickness of 5.7 ± 0.9 nm; the scale bar is 10 nm). B) Lattice planes imaged parallel to the edge of a Mn_3O_4 NP correlating with a (200) *d*-spacing value of 0.288 nm (Inset: optical diffractogram). C) Selected area electron diffraction (SAED) pattern showing clear diffraction rings indexed to the Mn_3O_4 spinel structure.

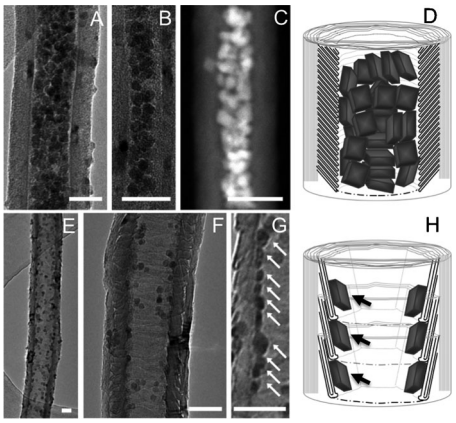

Figure 3. TEM images of Mn_3O_4@CNF (A–C) and Mn_3O_4@GNF (E–G). Dense packing of NP in Mn_3O_4@CNF, as revealed by bright field TEM (A-B) and high-angle annular dark-field scanning TEM (HAADF STEM) (C). Bright-field TEM images of Mn_3O_4 nanobricks adsorbed on the step-edges of GNF (E–G). The scale bars are 40 nm. Schematic diagrams illustrating Mn_3O_4 NP densely packed in a CNF (D) and sparsely distributed within a GNF through anchoring to the graphitic step-edges (H).

Table 1: Summary of the assembly of Mn_3O_4 NPs in host CNF and GNF nanocontainers and magnetic parameters for non-encapsulated nanobricks, Mn_3O_4@CNF and Mn_3O_4@GNF.

	Mn_3O_4 NP	Mn_3O_4@CNF	Mn_3O_4@GNF
packing density	–	high	low
NP–NP interaction	–	high	low
orientation	–	random	aligned
$T_{ZFC\text{-}peak}$ [K]	35.2	38.2	35.8
T_B (max of χ'' peak) [K]	31.6	35.7	31.9
M_{2K} [emu g^{-1}][a]	9.0	1.9	0.9
H_c at 2 K [T][a]	2.06	1.20	0.99
	symmetric (−1.02/ +1.04)	symmetric (−0.60/ +0.60)	asymmetric (−0.18/ +0.81)

[a] *M* is the magnetization value and H_c is the coercive field value both at 2 K.

a consequence of the encapsulation, a shift of the Mn–O vibrations was observed in the IR spectra for both Mn_3O_4@CNF and Mn_3O_4@GNF composites (Figure S13). While no preferential orientation of the nanobricks was observed for Mn_3O_4@CNF (Figure 3A–D), Mn_3O_4 NPs in GNFs appeared to be positioned with their largest facet parallel to the surface of the GNF step-edge (Figure 3F–G). It is considered that this preferential orientation of Mn_3O_4 NPs in GNFs is driven by a requirement to maximize host–guest interactions combined with a reduction of the NP surface area exposed to the environment. TEM imaging showed that after the removal of externally absorbed NPs from Mn_3O_4@CNF and Mn_3O_4@GNF the vast majority (about 95%) of the remaining Mn_3O_4 NPs were indeed encapsulated inside the nanofibers. A close inspection of Mn_3O_4@CNF revealed that for certain internal diameters of the nanofibers (about 27 nm), a highly ordered close-packed arrangement of the nanobricks was formed (Figure 3B).

The effect of the host-nanocontainer on the NP assemblies can be observed in the magnetic behavior of the resultant hybrid materials, with a decrease of the ZFC-FC splitting temperature in the following order: non-encapsulated Mn_3O_4 > Mn_3O_4@CNF > Mn_3O_4@GNF (Figure 4A), which correlates with the decreasing degree of aggregation of the nanobricks as observed by TEM. Furthermore, the higher magnetization value found at 2 K for Mn_3O_4@CNF as compared to Mn_3O_4@GNF (Figure 4B and Table 1) is in accordance with the TGA observations indicating a higher packing density for Mn_3O_4@CNF. The fact that the magnetic behavior of Mn_3O_4@GNF differs from the non-encapsulated NPs suggests that magnetic interactions cannot be attributed solely to core–shell interactions.[23] Since interparticle interactions for Mn_3O_4@GNF are expected to be much lower, the ferromagnetic contribution observed for non-encapsulated Mn_3O_4 NP is mainly due to dipole interactions. Comparison of the hysteresis curves (Figure 4C–D) supports this point further. For Mn_3O_4@GNF the magnetization reaches a saturation value at magnetic fields higher than 2 T, whereas for free Mn_3O_4 NPs and Mn_3O_4@CNF the magnetization value is still far from saturation even at 5 T.

As a consequence of encapsulation, the Mn_3O_4 nanobricks showed lower coercivity values. In contrast to Mn_3O_4@CNF, Mn_3O_4@GNF exhibited a nonsymmetrical hysteresis loop (Figure 4C). Close inspection revealed a fast-relaxation process close to zero-field (Figure 4D). Interestingly, this process became more pronounced at 300 K, where both non-encapsulated NPs (Figure S6) and empty nanofibers showed no magnetic ordering (Figure S15). The defects in the graphene layers of the step-edges in GNFs may provide a mechanism for this unusual ferromagnetic behavior observed for Mn_3O_4@GNF.[28,29] In contrast to the sigmoidal variation observed for Mn_3O_4@CNF, a rapid increase of the first magnetization curve (< 0.5 T) was found for Mn_3O_4@GNF suggesting that the easy magnetic axes of these nanobricks were distributed with some degree of preferred orientation, in agreement with the TEM observations showing the large facets of the nanobricks aligned with the GNF step-edge surfaces (Figure 3G).

Both the Mn_3O_4@GNF and Mn_3O_4@CNF hybrid nanostructures showed a frequency dependence of the out-of-phase (χ'') signal, typical of a spin glass-like behavior (Figures S16–19). However, the χ' peak maximum for Mn_3O_4@CNF was shifted to higher temperatures with respect to those found for Mn_3O_4@GNF and Mn_3O_4 (Figure 4E and Table 1). Both magnetic parameters T_B and $T_{ZFC\text{-}peak}$ showed the same trend. Careful statistical analysis of the size distribution of the encapsulated NP showed that slightly bigger nanobricks were preferentially encapsulated in CNF (Figure 4F and Table S1), explaining this observed increase in the blocking temperature (T_B; Figures S16 and S18).[30] While GNFs absorb NPs indiscriminately from solution, it is evident that the CNF cavities exhibit a clear preference for larger nanobricks whereby both host–guest and interparticle interactions are maximized.

In summary, we have developed an effective methodology for the integration of preformed magnetic NPs into the internal cavity of carbon

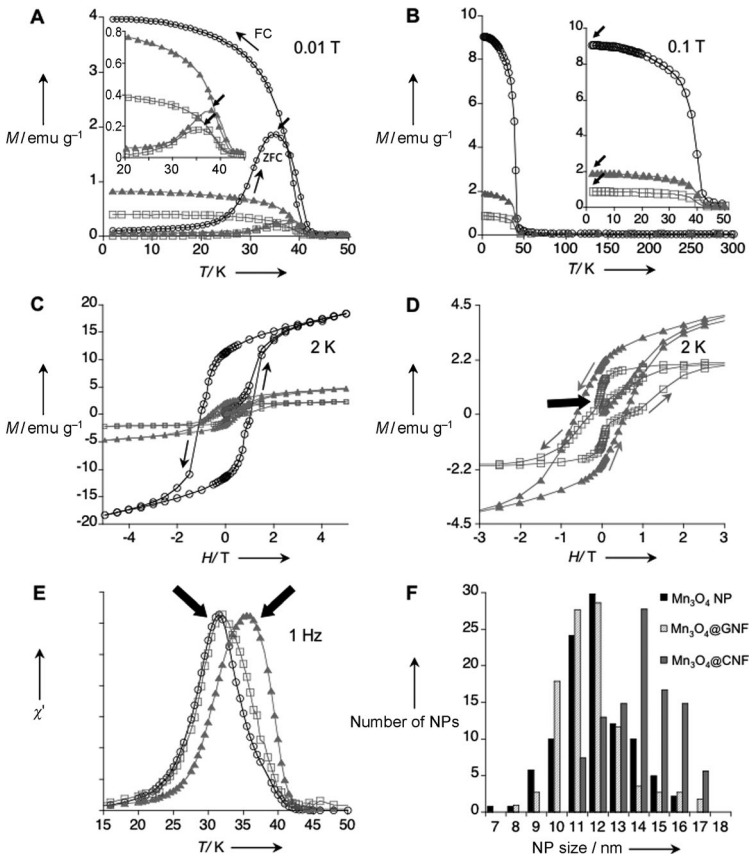

Figure 4. Magnetic measurements (A–E) and statistical analysis of the NP size (F) for non-encapsulated Mn_3O_4 NP (black ○), Mn_3O_4@CNF (red ▲), and Mn_3O_4@GNF (blue □). A) ZFC and FC (0.01 T) measurements. Inset: detail of the ZFC-FC splitting for Mn_3O_4@CNF and Mn_3O_4@CNF. B) Thermal variation of magnetization under an applied magnetic field of 0.1 T. Inset: expanded region 0–50 K. C,D) Magnetization curves (*M* vs. *H*) at 2 K. E) Comparison of the in-phase χ' susceptibility at 1 Hz.

nanofibers, yielding two different hybrid nanostructures exhibiting different magnetic behaviors (Table 1). The arrangement of NPs is precisely controlled by the internal structure of the host NF. Non-covalent interactions, which are responsible for the efficient transport and encapsulation of guest-NPs into NFs, in principle could allow NPs to stay mobile within the NFs and reversibly align along an applied magnetic field. The encapsulation of magnetic NPs into NFs described in this study opens up a number of exciting opportunities for applications requiring the precise control of position and orientation of guest-NPs, for example, nanoelectronics and nanocatalysis.[31,32] This new class of hybrid nanomaterial may enable the development of supercapacitors and facilitate harnessing of the synergistic effects of carbon host-nanofibers combined with the magnetic properties of guest-NP, which are important for the emerging area of spintronic devices.

Received: September 28, 2012
Published online: January 10, 2013

Keywords: carbon nanotubes · encapsulation · nanoparticles · self-assembly

[1] D. V. Talapin, E. V. Shevchenko, H. Weller, *Synthesis and Characterization of Magnetic Nanoparticles, Nanoparticles* (Ed.: G. Schmid), Wiley-VCH, Weinheim, **2001**.
[2] C. M. Sorensen, *Magnetism, Nanoscale Materials in Chemistry* (Ed.: K. J. Klabunde), Wiley-VCH, Weinheim, **2001**.
[3] T. W. Chamberlain, M. C. Gimenez-Lopez, A. N. Khlobystov, *Carbon Nanotubes and Related Structures: Synthesis Characterization, Functionalization and Applications* (Ed.: D. M. Guldi, N. Martin), Wiley-VCH, Weinheim, **2010**.
[4] M. C. Gimenez-Lopez, F. Moro, A. La Torre, C. Gómez-Garcia, P. D. Brown, J. van Slageren, A. N. Khlobystov, *Nat. Commun.* **2011**, *2*, 407.
[5] L. Guan, Z. Shi, M. Li, Z. Gu, *Carbon* **2005**, *43*, 2780 – 2785.
[6] U. Ugarte, A. Chatelain, W. A. De Heer, *Science* **1996**, *274*, 1897 – 1899.
[7] Y. A. Koksharov, *Magnetism of Nanoparticles: Effects of Size, Shape and Interactions, Magnetic Nanoparticles* (Eds.: S. P. Gubin), Wiley-VCH, Weinheim, **2009**.
[8] M. Zhu, G. Diao, *Nanoscale* **2011**, *3*, 2748 – 2767.
[9] A. La Torre, G. A. Rance, J. El Harfi, J. Li, D. J. Irving, P. D. Brown, A. N. Khlobystov, *Nanoscale* **2010**, *2*, 1006 – 1010.
[10] A. La Torre, M. W. Fay, G. A. Rance, M. C. Gimenez-Lopez, W. A. Solomonsz, P. D. Brown, A. N. Khlobystov, *Small* **2012**, *6*, 1 – 7.
[11] E. Castillejos, P.-J. Debouttiere, L. Roiban, A. Solhy, V. Martinez, Y. Kihn, O. Ersen, K. Philippot, B. Chaudret, P. Serp, *Angew. Chem.* **2009**, *121*, 2567 – 2571; *Angew. Chem. Int. Ed.* **2009**, *48*, 2529 – 2533.
[12] J. V. I. Timonen, E. T. Seppälä, O. Ikkala, R. H. A. Ras, *Angew. Chem.* **2011**, *123*, 2128 – 2132; *Angew. Chem. Int. Ed.* **2011**, *50*, 2080 – 2084.
[13] P. Guardia, J. Perez-Juste, A. Labarta, X. Batlle, L. M. Marzan, *Chem. Commun.* **2010**, *46*, 6108 – 6110.
[14] K. J. M. Bishop, C. E. Wilmer, S. Soh, B. A. Grzybowski, *Small* **2009**, *5*, 1600 – 1630.
[15] T. Yu, J. Moon, J. Park, Y. Park, H. B. Na, B. H. Kim, I. C. Song, W. K. Moon, T. Hyeon, *Chem. Mater.* **2009**, *21*, 2272 – 2279.
[16] X. Li, L. Zhou, J. Gao, H. Miao, H. Zhang, J. Xu, *Powder Technol.* **2009**, *190*, 324 – 326.
[17] G. An, P. Yu, M. Xiao, Z. Liu, Z. Miao, K. Ding, L. Mao, *Nanotechnology* **2008**, *19*, 275709.
[18] W. Chen, Z. Fan, L. Gu, X. Bao, C. Wang, *Chem. Commun.* **2010**, *46*, 3905 – 3907.
[19] D. Yan, S. Cheng, R. F. Zhuo, J. T. Chen, J. J. Feng, H. J. Li, Z. G. Wu, J. Wang, P. X. Yan, *Nanotechnology* **2009**, *20*, 105706.
[20] M. Rajamathi, M. Ghosh, R. Seshadri, *Chem. Commun.* **2002**, 1152 – 1153.
[21] G. Srinivasan, M. S. Seehra, *Phys. Rev. B* **1983**, *28*, 1 – 7.
[22] G. B. Jensen, *J. Phys. C* **1974**, *7*, 409 – 424.
[23] K. Dwight, N. Menyuk, *Phys. Rev.* **1960**, *119*, 1470 – 1479.
[24] F. Jiao, A. Harrison, P. G. Bruce, *Angew. Chem.* **2007**, *119*, 4020 – 4024; *Angew. Chem. Int. Ed.* **2007**, *46*, 3946 – 3950.
[25] N. Wang, L. Guo, L. He, X. Cao, C. Chen, R. Wang, S. Yang, *Small* **2007**, *3*, 606 – 610.
[26] S. Shtrikman, E. P. Wohlfarth, *Phys. Lett. A* **1981**, *85*, 467 – 470.
[27] J. L. Dormann, F. D'orazio, F. Lucari, E. Tronc, P. Prene, J. P. Jolivet, D. Fiorani, R. Cherkaoui, M. Nogues, *Phys. Rev. B* **1996**, *53*, 14291 – 14297.
[28] S. Ma, J. H. Xia, V. V. S. S. Srikanth, X. Sun, T. Staedler, X. Jiang, F. Yang, Z. D. Zhang, *Appl. Phys. Lett.* **2009**, *95*, 263105.
[29] P. Esquinazi, D. Spemann, R. Höhne, A. Setzer, K. H. Han, T. Butz, *Phys. Rev. Lett.* **2003**, *91*, 227201.
[30] W. S. Seo, H. H. Jo, K. Lee, B. Kim, S. J. Oh, J. T. Park, *Angew. Chem.* **2004**, *116*, 1135 – 1137; *Angew. Chem. Int. Ed.* **2004**, *43*, 1115 – 1117.
[31] A. N. Khlobystov, *ACS Nano* **2011**, *5*, 9306 – 9312.
[32] P. V. Dudin, P. R. Unwin, J. V. Macpherson, *Phys. Chem. Chem. Phys.* **2011**, *13*, 17146 – 17152.

